

FULL EXPLOITATION OF WAVELET COEFFICIENTS IN RADAR IMAGING FOR IMPROVING THE DETECTION OF A CLASS OF SOURCES IN THE CONTEXT OF REAL DATA

M. Tria[†] J.P. Ovarlez[†] L. Vignaud[†] J.C. Castelli[†] and M. Benidir[‡]

[†] LIS-ENSIEG, BP 46, 38402 Saint Martin d'Hres, France

[†] ONERA, DEMR, BP 72, 92322 Chatillon, France

[‡] L.S.S. (UMR 8506), Supelec, 91192 Gif-sur-Yvette cedex, France

email : tria@lis.inpg.fr, ovarlez@onera.fr, vignaud@onera.fr,
castelli@onera.fr, benidir@lss.supelec.fr

ABSTRACT

As a time-frequency tool, the Continuous Wavelet Transform (CWT) was applied in radar imaging to reveal that the reflectors' response varies as a function of frequency f and aspect angle θ (orientation of the wave vector). To do so, we constructed a hyperimage expressed as the squared modulus of the wavelet coefficients, allowing to access to the energy distribution of each reflector, in the $f - \theta$ plane.

Exploiting the hyperimage, our recent researches were devoted to the classification of the reflectors in function of their energy distributions with the objective of discriminating a type of target in the radar image. Although acceptable results were obtained, the method is not reliable in some cases.

The purpose of this paper is to show that exploiting not only the modulus but also the argument of the wavelet coefficients, can improve the detection of a certain class of reflectors. Results are presented at the end of this article.

Keywords : Time-Frequency Analysis, Continuous Wavelet Transform, Nonstationary Signal, Radar Imaging, Detection, Source Classification, Target Extraction.

1. PRINCIPLE OF SAR IMAGING

The SAR (Synthetic Aperture Radar) imaging process consists in the formation of high resolution images. To do so, a moving radar emits pulses and collects the elementary signals reflected by scatterers. Once the overall SAR signal is stored, the high-resolution image is obtained by Fourier-based techniques [1, 2, 3]. The SAR images analysed in this paper are formed with the radar RAMSES [4] at the ONERA.

As shown in figure 1, the imaging plane is labelled using an $x - y$ Cartesian coordinate system with origin at a reference point O . We assume that the radar moves in a straight line and in a direction parallel to the cross-range direction. The radar position is described by the azimuth angle θ defined counter clockwise from the y direction. Moreover, we suppose far zone backscatter, and therefore we obtain plane-wave incidence on objects. In addition, we assume high-frequency radar measurements and consequently the scattering response of a man-made target is well approximated as

a sum of responses from individual scatterers. If the radar measurements are carried out over a broad bandwidth and a wide angular window of observation, we have to consider a model that takes the scattering phenomenology into account. For a given polarisation, this scattering model is expressed as a summation of point scatterers multiplied by their respective frequency and aspect dependent complex amplitude $\sigma_i(f, \theta)$:

$$H(\vec{k}) = \sum_{i=1}^{i=N} \sigma_i(f, \theta) \exp(-j2\pi\vec{k} \cdot \vec{r}_i) \quad (1)$$

where \vec{k} is the wave vector in the direction of the scattered field:

$$\vec{k} = \begin{pmatrix} k_x \\ k_y \end{pmatrix} = \begin{pmatrix} k \cos(\theta) \\ k \sin(\theta) \end{pmatrix}$$

where $k = 2f/c$ is the wave number with f the frequency and c the speed of light, θ corresponds to the observation aspect (see figure 1). The position vector is $\vec{r} = (x, y)^T$ where x and y represent the slant-range and cross-range locations.

Referring to the Geometrical Theory of Diffraction (GTD) [5, 6], the aspect and frequency dependent response $|\sigma_i(f, \theta)| = A_i(f, \theta)$ is a 2D-function determined by the geometry, composition and orientation of the scattering mechanism. Indeed, the GTD predicts that the response $A_i(f, \theta)$ depends also on a set of parameters $\{\gamma_i, L_i, \theta_i\}$ describing the shape, the length and the orientation of the scatterer, respectively. We can also suppose that the argument of $\sigma_i(f, \theta)$ depends on frequency and aspect θ : $\arg[\sigma_i(f, \theta)] = \phi_i(f, \theta)$. A scatterer is said *colored* and *anisotropic* if its response $|\sigma_i|$ depends on the frequency f and the aspect θ , respectively. To highlight the coloration and the anisotropy of the scatterers, we suggested the use of a method based on the Continuous Wavelet Transform (CWT) that is a particular tool of the time-frequency analysis.

2. CONSTRUCTION OF HYPERIMAGES USING THE CWT

To access to the energy distribution of the scatterers, in the $f - \theta$ plane, we constructed the concept of hyperimage which expresses as the squared modulus of the wavelet

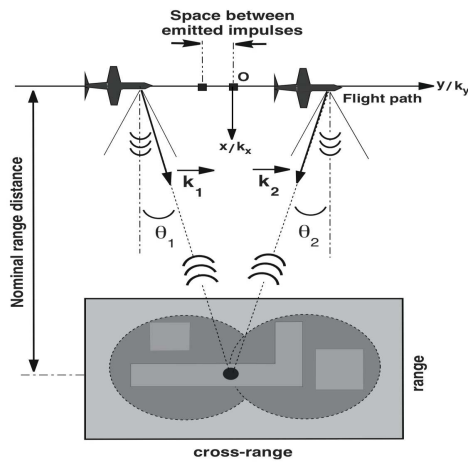


Figure 1: Illustration of a scatterer irradiated at two different aspect angles (i.e. two different positions of the moving radar) in SAR imaging.

coefficients divided by the admissibility wavelet coefficient A_ϕ [7, 8]:

$$I_H(\vec{r}_o, \vec{k}_o) = \frac{1}{A_\phi} \left| W_H(\vec{r}_o, \vec{k}_o) \right|^2 \quad (2)$$

By noting ϕ the mother wavelet localised around $(k, \theta) = (1, 0)$, the admissibility coefficient A_ϕ is defined as:

$$A_\phi = \int \frac{|\phi(\vec{k})|^2}{k^2} d\vec{k} < \infty. \quad (3)$$

The wavelet coefficients $W_H(\vec{r}_o, \vec{k}_o)$ are introduced as the scalar product between the backscattering signal H and each wavelet $\Psi_{\vec{r}_o, \vec{k}_o}$:

$$W_H(\vec{r}_o, \vec{k}_o) = \int H(\vec{k}) \Psi_{\vec{r}_o, \vec{k}_o}^*(\vec{k}) d\vec{k}$$

where the family of wavelets $\Psi_{\vec{r}_o, \vec{k}_o}(\vec{k})$ are generated from the mother wavelet $\phi(\vec{k})$ by rotation \mathcal{R}_{θ_o} , translation \vec{r}_o and contraction with the scale factor $1/k_o$ according to:

$$\begin{aligned} \Psi_{\vec{r}_o, \vec{k}_o}(\vec{k}) &= \frac{1}{k_o} e^{-2i\pi\vec{k}\cdot\vec{r}_o} \phi\left(\frac{1}{k_o} \mathcal{R}_{\theta_o}^{-1} \vec{k}\right) \\ &= \frac{1}{k_o} e^{-2i\pi\vec{k}\cdot\vec{r}_o} \phi\left(\frac{k}{k_o}, \theta - \theta_o\right). \end{aligned} \quad (4)$$

The wavelet coefficients $W_H(\vec{r}_o, \vec{k}_o)$ express literally as :

$$\begin{aligned} W_H(\vec{r}_o, \vec{k}_o) &= \int_0^{2\pi} d\theta \int_0^{+\infty} k H(k, \theta) \\ &\quad \frac{1}{k_o} e^{j2\pi\vec{k}\cdot\vec{r}_o} \phi^*\left(\frac{k}{k_o}, \theta - \theta_o\right) dk \end{aligned} \quad (5)$$

2.1 Interpretation of the hyperimage $I(\vec{r}, \vec{k})$

Let us rewrite $I(\vec{r}, \vec{k}) \equiv I(x, y; f, \theta)$. For each reflector located at $\vec{r}_o = (x_o, y_o)$, we can extract its energy distribution $I(x_o, y_o; f, \theta)$, in the $f - \theta$ plane. Examples of energy distribution corresponding to real target reflectors can be found in [9, 10, 11].

3. IMPROVING THE DETECTION OF A REFLECTOR CLASS BY EXPLOITING THE FULL INFORMATION OF WAVELET COEFFICIENTS

The basic idea we proposed is to select among all the scatterers' energy distributions, one energy distribution susceptible to be characteristic of the type of object to be discriminated : this distribution becomes a reference one. Then, the purpose is to identify the scatterers in the image that have similar distributions to the reference one. We call *object* a structure with a unique and simple geometry (edge, cylinder, flat plate, ...). The algorithm has consisted in selecting a pixel located at (x_{ref}, y_{ref}) in the SAR image, with the help of a visual interface called i4d (see figure 2), and correlating its corresponding distribution $I(x_{ref}, y_{ref}; f, \theta) \equiv I_{ref}(f, \theta)$ with the distributions $I(x_i, y_j; f, \theta) \equiv I_{i,j}(f, \theta)$ corresponding to the others pixels $P_{i,j}$ located at (x_i, y_j) in the SAR image, respectively :

$$C_{ref}(x_i, y_j) = \frac{\int I_{ref}(f, \theta) I_{i,j}(f, \theta) df d\theta}{\sqrt{E_{ref}} \sqrt{E_{i,j}}} \quad (6)$$

where $E_{i,j}$ and E_{ref} are normalised terms, defined as :

$$\begin{aligned} E_{i,j} &= \int |I(x_i, y_j; f, \theta)|^2 df d\theta. \\ E_{ref} &= \int |I(x_{ref}, y_{ref}; f, \theta)|^2 df d\theta. \end{aligned}$$

The figure 2 describes the use of a visual interface called i4d, for selecting a pixel located at (x_o, y_o) in the plane (x, y) , with sliders (see the above plot) and visualizing the corresponding wavelet coefficient $W(x_o, y_o; f, \theta)$ in modulus (see the below left plot) and in phase (see the below right plot). The initial SAR image $I(x, y)$ is displayed inside the x - y plane, in order that the user be sure that the pixel he selects, corresponds to a reflector belonging to the object to be discriminated.

In some SAR images that we analysed, this algorithm proved its efficiency to discriminate a type of object [11, 12, 13]. Unfortunately, the above method is not reliable in some cases. Recalling that the energy distribution $I(x, y; f, \theta)$ expresses from the squared modulus of the wavelet coefficients, the present work consists in exploiting not only the modulus but also the phase of the wavelet coefficients, which is also susceptible to characterise the reflectors. The full exploitation of wavelet coefficients was carried out within the framework of Polarimetry and Interferometry with good results in terms of target classification and target height estimation [14].

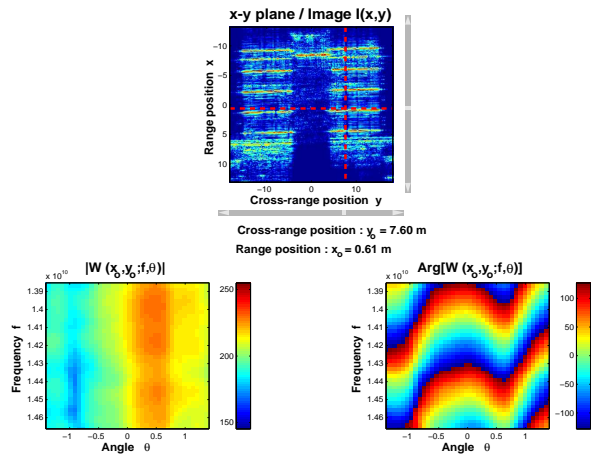


Figure 2: Presentation of the visual interface i4d : visualisation of the wavelet coefficient $W(x_o, y_o; f, \theta)$ (in modulus and in phase), corresponding to the selected pixel located at (x_o, y_o) .

Consequently, in order to improve the object extraction, the function in equation (6) is replaced by :

$$C'_{ref}(x_i, y_j) = \frac{\int W_{ref}(f, \theta) W_{i,j}^*(f, \theta) df d\theta}{\sqrt{E'_{ref}} \sqrt{E'_{i,j}}} \quad (7)$$

where $E'_{i,j}$ and E'_{ref} are defined as :

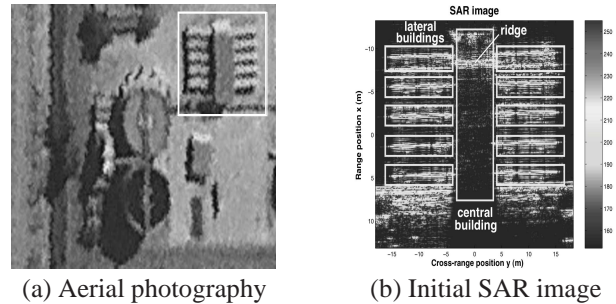
$$E'_{i,j} = \int |W(x_i, y_j; f, \theta)|^2 df d\theta.$$

$$E'_{ref} = \int |W(x_{ref}, y_{ref}; f, \theta)|^2 df d\theta.$$

4. RESULTS

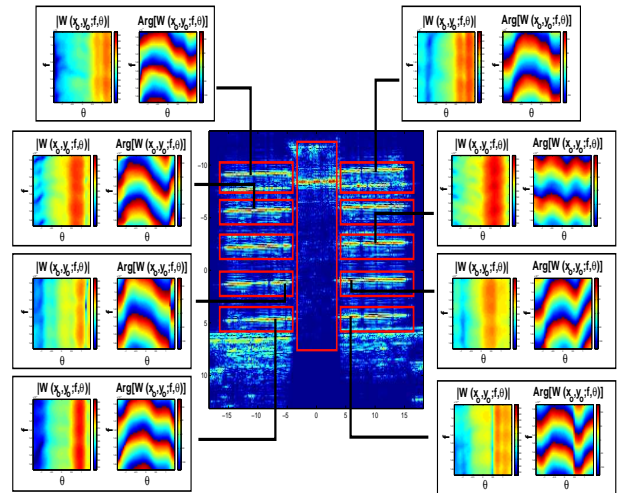
The analysed SAR image is composed of a warehouse : lateral buildings are attached to a big one on both sides (see figures 3 (a) and 3 (b)). In the figure 3 (c), we select some pixels P_o located at (x_o, y_o) on the lateral buildings (as described in the figure 2) and we illustrate the corresponding wavelet coefficients $W(x_o, y_o; f, \theta)$ (represented in modulus and phase), in the $f - \theta$ plane : we can observe that these wavelet coefficients present some similarities especially in phase.

Here, our objective is to show that making correlation between the wavelet coefficients (see equation (7)) and a reference one, can be more efficient than correlating only the modulus of them with a reference one (see equation (6)) in terms of object extraction. In order to extract the lateral buildings, we select a pixel located on one lateral building and consider its corresponding wavelet coefficient as the reference one. The figure 4 (a) shows the location of the reference pixel P_{ref} located at (x_{ref}, y_{ref}) and illustrates the corresponding wavelet coefficient $W(x_{ref}, y_{ref}; f, \theta)$ (represented in modulus and phase). The figures 4 (b) and 4 (c) illustrate the correlation map corresponding to the reference pixel and



(a) Aerial photography

(b) Initial SAR image



(c) Wavelet coefficients (represented in modulus and phase) corresponding to some pixels located on the lateral buildings.

Figure 3: We reveal that the wavelet coefficients corresponding to the analysed pixels present some similarities (especially in phase).

resulting from equation (6) and equation (7), respectively. To visualize the sources detected, in 1D, we can propose to plot different cross-sections of the correlation maps, along the y -axis. But, in order that the 1D visualization be representative of the correlation maps in figures 4 (b) and 4 (c), we have proposed to average the cross-sections along the x -axis, within a neighbourhood \mathcal{N}_{x_o} around the range position x_o :

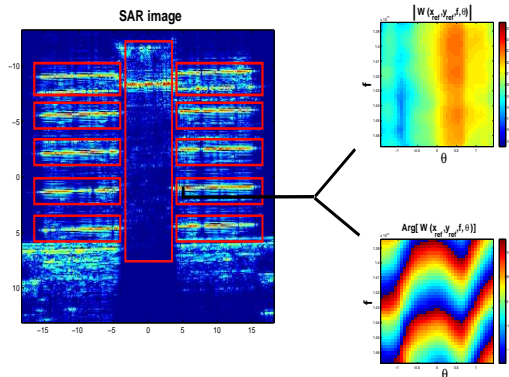
$$\bar{C}_{ref}^{(x_o)}(y) = \sum_{x_i \in \mathcal{N}_{x_o}} C_{ref}(x_i, y) \quad (8)$$

$$\bar{C}'_{ref}{}^{(x_o)}(y) = \sum_{x_i \in \mathcal{N}_{x_o}} C'_{ref}(x_i, y) \quad (9)$$

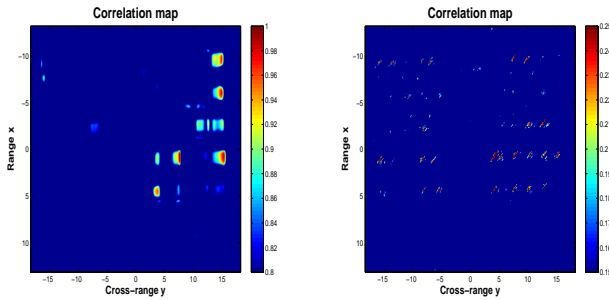
where $\mathcal{N}_{x_o} = \{x_i / x_i \in [x_o - \delta, x_o + \delta]\}$. The plots of $\bar{C}_{ref}^{(x_o)}(y)$ (blue color) and $\bar{C}'_{ref}{}^{(x_o)}(y)$ (red color) are displayed in the figures 5 (a), 5 (b) and 5 (c) for $x_o = -9.6$ m, $x_o = 0.9$ m and $x_o = 4.1$ m, respectively.

We can notice that the lateral buildings are extracted better in the figure 4 (c) than in the figure 4 (b). Precisely, two kinds of improvement are obtained with the exploitation of the full information of wavelet coefficients : first, more reflectors composing the lateral buildings are detected, especially those ones localised on the left-hand buildings (see

figures 4 (b), 4 (c) and figures 5 (a) to (c); secondly, the localization of the reflectors detected, is more accurate (see figures 5 (a) to (c)).



(a) Choice of the reference pixel P_{ref} located at (x_{ref}, y_{ref}) on one lateral building and representation of $W(x_{ref}, y_{ref}; f, \theta)$ in modulus and phase.

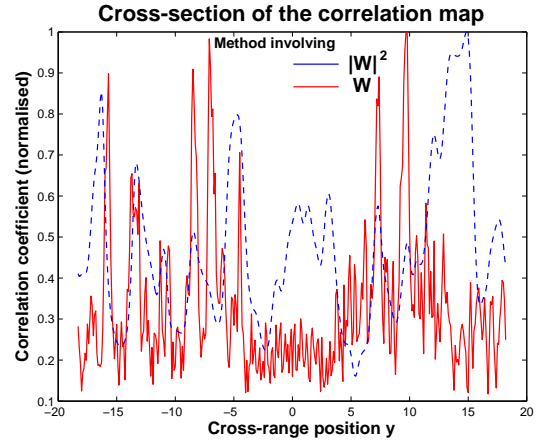


(b) $C_{ref}(x, y)$: correlation between the energy distributions and the reference one I_{ref} .
 (c) $C'_{ref}(x, y)$: correlation between the wavelet coefficients and the reference one W_{ref} .

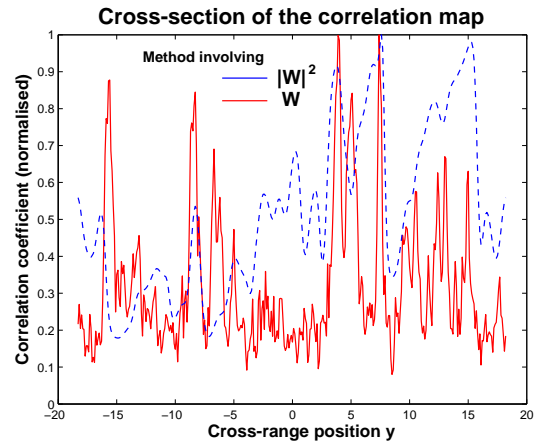
Figure 4: Improvement of the lateral buildings extraction by correlating the wavelet coefficients with W_{ref} .

5. CONCLUSION AND PERSPECTIVES

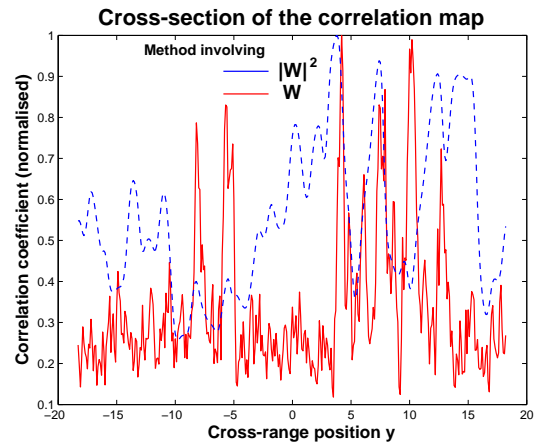
By considering not only the modulus but also the argument of the wavelet coefficients, we obtain a better characterisation of each reflector. By analysing some reflectors localised on the lateral buildings, we observe that the corresponding wavelet coefficients present some similarities especially in phase. These observations lead us to correlate the wavelet coefficients for improving the detection of the reflectors belonging to the lateral buildings. Comparing with the method exploiting only the squared modulus of the wavelets coefficients, we notice that the extraction of the lateral buildings is improved. Moreover, the method proposed in this paper seems to be robust to noise : thorough studies in simulation have to be made to confirm the robustness to noise.



(a) 1D visualisation around $x_o = -9.6$ m : seven sources are detected with the method involving the wavelet coefficients.



(b) 1D visualisation around $x_o = 0.9$ m : at least, six sources are detected with the method involving the wavelet coefficients.



(c) 1D visualisation around $x_o = 4.1$ m : at least, five sources are detected with the method involving the wavelet coefficients.

Figure 5: Cross-sections of the correlation map and comparison of the methods involving the squared modulus and the full information of wavelet coefficients, respectively.

As perspectives, we can propose to apply this new method to other SAR images in order to see if the targets composing these images can be successfully extracted. Again, a comparison with the method involving the squared modulus of the wavelet coefficients must be envisaged. The reference wavelet coefficient can be obtained leaning on a priori information concerning the object to be extracted; for example, the theory of diffraction provides frequency and aspect dependent responses of canonical objects (flat plate, cylinder, edge, ...). In addition, the method can be easily applied to others 1-D nonstationary physical signals (radar, sonar, seismic, acoustic, sound, ...) with the aim of classifying the different sources. Finally, separation source methods could be applied to SAR signals and compared with the previous wavelet based-algorithm in terms of target extraction.

REFERENCES

- [1] M. Soumekh, *Fourier Array Imaging*, PTR Prentice Hall (1994), Englewood Cliffs.
- [2] M. Soumekh, *Synthetic Aperture Radar Signal Processing*, John Wiley & Sons, Inc (April 1999).
- [3] P.T. Gough D.W. Hawkins, Unified Framework for Modern Synthetic Aperture Imaging Algorithms, *Int. J. of Imaging Systems and Technology*, **8** (1997), 343-358.
- [4] J.M. Boutry, ONERA Airborne SAR Facilities, *2nd International Airborne Remote Sensing Conference* (June 1996), San Francisco, USA.
- [5] L.C. Potter D.M. Chiang R. Carrire and M.J. Gerry, A Geometrical Theory of Diffraction (GTD)-Based Parametric Model for Radar Scattering, *IEEE Trans. On Antennas and Propagation*, **43** (Oct. 1995), 1058-1067.
- [6] L.C. Potter and R.L. Moses, Attributed Scattering Centers for SAR ATR, *IEEE Trans. On Image Processing*, **6** (Jan. 1997), 79-91.
- [7] J. Bertrand P. Bertrand and J.P. Ovarlez, Dimensionalized Wavelet Transform with Application to Radar Imaging, *Proc. IEEE-ICASSP* (May 1991), Toronto, Canada.
- [8] J. Bertrand P. Bertrand and J.P. Ovarlez, Frequency Directivity Scanning in Laboratory Radar Imaging, *Int. J. of Imaging Systems and Technology*, **5** (1994), 39-51.
- [9] J.P. Ovarlez L. Vignaud J.C. Castelli M. Tria and M. Benidir, Analysis of SAR Images by Multidimensional Wavelet Transform, *IEE-Radar, Sonar and Navigation- Special Issue On Time-Frequency Analysis for Synthetic Aperture Radar and Feature Extraction*, **150**(4) (august 2003), 234-241.
- [10] M. Tria J.P. Ovarlez L. Vignaud J.C. Castelli and M. Benidir, SAR imaging using multidimensional continuous wavelet transform, *Proc. Eusipco'04, European Signal Processing Conference* (Sept. 2004), Vienna-Austria.
- [11] M. Tria, *Imagerie Radar à Synthèse d'Ouverture Par Analyse en Ondelettes Continues Multidimensionnelles*, Ph. Doctorate, University of Paris XI (2005).
- [12] M. Tria J.P. Ovarlez L. Vignaud J.C. Castelli and M. Benidir, The multidimensional continuous wavelet transform in SAR imaging, a tool for the object classification, *Proc. Radar'04, International Conference on Radar Systems* (Oct. 2004), Toulouse-France.
- [13] M. Tria J.P. Ovarlez L. Vignaud J.C. Castelli and M. Benidir, Extracting Real Objects in Radar Imaging by Exploiting the Squared Modulus of the Continuous Wavelet Transform, accepted subject to revisions *IEE, Radar, Sonar and Navigation*.
- [14] E. Colin, M. Tria, C. Titin-Schneider, J.P. Ovarlez and M. Benidir, SAR Imaging Using The Multidimensional Continuous Wavelet Transform and Applications to Polarimetry and Interferometry, *International Journal of Imaging Systems and Technology*, **14**, Issue 5, 206-212.